Applied Physics Express



# GaN-based MIS-HEMTs with $Al_2O_3$ dielectric deposited by low-cost and environmental-friendly mist-CVD technique

OPEN ACCESS

Applied Physics Express 14, 031004 (2021) LETTER

https://doi.org/10.35848/1882-0786/abe19e

# GaN-based MIS-HEMTs with $Al_2O_3$ dielectric deposited by low-cost and environmental-friendly mist-CVD technique

Rui Shan Low[1], Joel T. Asubar[1*], Ali Baratov[1], Shunsuke Kamiya[1], Itsuki Nagase[1], Shun Urano[1], Shinsaku Kawabata[1], Hirokuni Tokuda[1], Masaaki Kuzuhara[2], Yusui Nakamura[3], Kenta Naito[3], Tomohiro Motoyama[3], and Zenji Yatabe[3*]

[1]University of Fukui, Fukui, 910-8507 Japan
[2]Kwansei Gakuin University, Hyogo, 662-8501 Japan
[3]Kumamoto University, Kumamoto, 860-8555 Japan

*E-mail: joel@u-fukui.ac.jp; yatabe@cs.kumamoto-u.ac.jp

Received December 17, 2020; revised January 14, 2021; accepted January 28, 2021; published online February 16, 2021

We report on the fabrication and characterization of AlGaN/GaN metal-insulator-semiconductor (MIS) capacitors and high-electron-mobility transistors (MIS-HEMTs) using a 5 nm thick $Al_2O_3$ dielectric deposited by cost-effective and environmental-friendly mist chemical vapor deposition (mist-CVD) technique. Practically hysteresis-free capacitance–voltage profiles were obtained from the fabricated two-terminal MIS-capacitors indicating high quality of the mist-$Al_2O_3$/AlGaN interface. Compared with reference Schottky-gate HEMTs, mist MIS-HEMTs exhibited much improved performance including higher drain current on-to-off ratio, much lower gate leakage current in both forward and reverse directions and lower subthreshold swing. These results demonstrate the potential and viability of non-vacuum mist-CVD $Al_2O_3$ in the development of high-performance GaN-based MIS-HEMTs. © 2021 The Japan Society of Applied Physics

The past few years have witnessed the AlGaN/GaN high-electron-mobility transistor (HEMT) delivering its promise of unmatched power levels and efficiencies.[1–3] From the view point of improved performance in terms of increased input dynamic range, significantly reduced leakage current, and added passivation effect, the metal-insulator-semiconductor (MIS) gate structure has been suggested to be an indispensable and a key structure for state-of-the-art GaN-based MIS-HEMTs.[3] Oxides such as $SiO_2$, $Al_2O_3$, $ZrO_2$, and $HfO_2$ have gained interest as candidate insulator materials for the MIS structure.[2] Among these, $Al_2O_3$ with its wide bandgap (~7 eV), high critical field (~10 MV $cm^{-1}$) and modest relative permittivity (~9), has received the most serious consideration.[4] High quality $Al_2O_3$ thin films are usually deposited using atomic layer deposition (ALD) and other deposition techniques under vacuum conditions.[5–11] It is reasonable to say that the ALD technique has paved the way for the manufacture of III–V MOSFETs, because it can provide high-grade oxides/III–V interfaces.[2]

Meanwhile, mist chemical vapor deposition (mist-CVD) technique has been steadily growing in popularity as an ecofriendly alternative approach for depositing oxide films.[12–14] The mist-CVD offers the merits of cost-effectiveness and environmental-friendliness since deposition is done under atmospheric pressure without any need for vacuum system, which can consume large amounts of energy.[14] Moreover, in ALD, highly pyrophoric trimethylaluminum (TMA) is usually used as the aluminum precursor. Since TMA can spontaneously ignite upon contact with air, it demands extensive safety precautions. On the other hand, mist CVD system employs far safer aluminum acetylacetonate as an aluminum source. Applications of high quality mist-CVD prepared $Al_2O_3$ in In–Ga–Zn–O thin film transistors[13] and silicon solar cells[15] have already demonstrated. Using mist-CVD, Yatabe et al., recently have reported excellent quality amorphous aluminum oxide films[16,17] whose properties are highly competitive against those prepared with the more sophisticated ALD method. Despite their promising potential as a gate insulator for GaN-based devices, surprisingly however, there have been no reports of AlGaN/GaN MIS-HEMTs using mist-CVD-prepared $Al_2O_3$ as gate dielectric, and therefore mist-$Al_2O_3$/AlGaN interfacial qualities remain to be unknown.

In view of the above, in this work, we report on the fabrication and characterization of AlGaN/GaN MIS-capacitors and transistors (MIS-HEMTs) using $Al_2O_3$ dielectric deposited by mist-CVD. To survey the quality of the resulting mist-$Al_2O_3$ and AlGaN interfaces, capacitance–voltage ($C$–$V$) measurements using Agilent 4284 A precision LCR meter were carried out. The experimentally obtained $C$–$V$ profiles were fitted to the disorder-induced gap state (DIGS) model,[18] using a rigorous one-dimensional simulation including consistent Poisson–Schrodinger calculations.[19,20] The performance of the MIS-HEMTs were then evaluated by current–voltage ($I$–$V$) measurements using Keysight B1505A power device analyzer/curve tracer.

The starting wafer used is a commercially available AlGaN/GaN heterostructure grown on SiC substrate by metal-organic vapor phase epitaxy. According to the data sheet, the AlGaN barrier layer has a nominal thickness ($d_{AlGaN}$) of 24 nm and Al composition $x$ of 0.25. The typical value of 2DEG sheet carrier density is $1 \times 10^{13}$ $cm^{-2}$ with mobility of 1510 $cm^2$ $V^{-1}$ $s^{-1}$. Figure 1 shows the schematic cross-section of mist- $Al_2O_3$/AlGaN/GaN MIS-capacitor and MIS-HEMT studied in this work. The device fabrication process was initiated with the formation of device isolation trenches by inductively coupled plasma reactive ion etching (ICP-RIE) using a gas mixture of $BCl_3/Cl_2$. This is followed by electron beam evaporation of Ti/Al/Mo/Au (15/60/35/50 nm) multi-stack for source/drain electrodes. After depositing a 30 nm thick SiN capping layer by sputtering, the metal multi-stack was alloyed by rapid thermal annealing (RTA) under $N_2$ atmosphere at 870 °C for 30 s for achieving good ohmic contact. During this high thermal budget RTA process, the AlGaN surface was protected by the SiN capping layer, to suppress nitrogen vacancies formation that is deleterious for

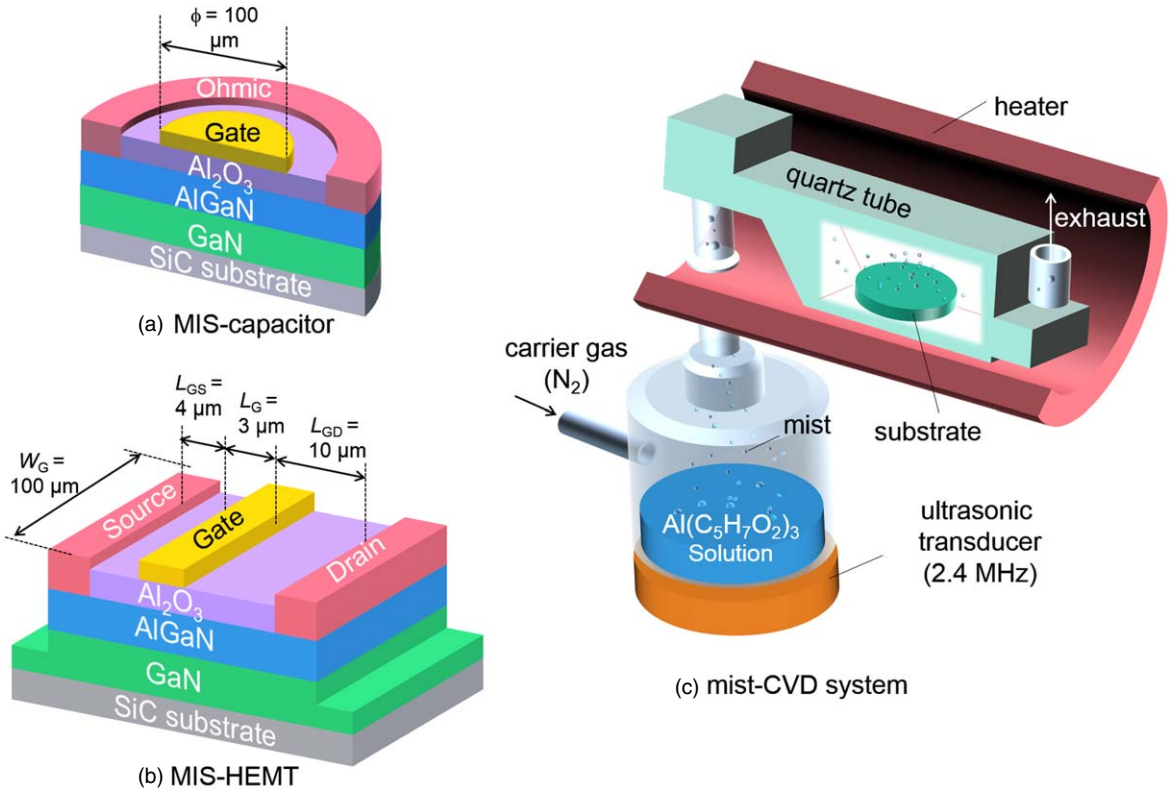


**Fig. 1.** (Color online) Schematic cross-section of mist-CVD $Al_2O_3$/AlGaN/GaN: (a) MIS-capacitor and (b) MIS-HEMT. (c) Schematic illustration of mist-CVD system used to deposit $Al_2O_3$ gate dielectric.

device operation.[21,22] The SiN cap was subsequently removed by buffered oxide etch solution of BHF and $NH_4F$. The samples then were immediately loaded to the quartz tube chamber of a home-made mist-CVD system[23] illustrated in Fig. 1(c) for the deposition of $Al_2O_3$ gate insulator.

Aluminum acetylacetonate [$Al(C_5H_7O_2)_3$] dissolved in methanol (99.8% purity MeOH) was used as the liquid precursor solution, which was atomized using a 2.4 MHz ultrasonic transducer. The generated Al-containing mist droplets were then transported by $N_2$ carrier gas to the deposition chamber containing the heated sample. During the entire deposition time of 90 s, the $N_2$ gas carrier flow rate was held constant at 3 l min$^{-1}$ while the sample temperature maintained at 400 °C. Further details of $Al_2O_3$ deposition is described elsewhere.[16]

After the formation of the $Al_2O_3$ gate dielectric, a Ni/Au (50/150 nm) bilayer stack for metal gate electrodes was deposited by electron beam deposition, concluding the fabrication process of mist-$Al_2O_3$/AlGaN/GaN MIS-capacitors and MIS-HEMTs. The fabricated MIS-capacitors have donut-shaped ohmic contacts concentric with the gate metal of 100 $\mu$m diameter, giving an effective capacitance area of $7.85 \times 10^{-5}$ cm$^2$ [see Fig. 1(a)]. For the MIS-HEMTs, the device gate length $L_G$, width $W_G$, gate-to-drain spacing $L_{GD}$, and gate-to-source spacing $L_{GS}$ were 3, 100, 10, and 4 $\mu$m, respectively [see Fig. 1(b)]. Schottky-gate AlGaN/GaN capacitors (SG-capacitors) and HEMTs (SG-HEMTs) were also fabricated for benchmarking purposes.

Since the quality of the mist-$Al_2O_3$ and AlGaN interfaces is of primary concern and critical for the performance of the resulting devices, we first investigated the $C$–$V$ characteristics of the MIS-capacitor samples. Figure 2(a) presents the dual-sweep $C$–$V$ profiles of the SG-capacitor and MIS-capacitor samples. The inset of the figure shows the carrier density profile computed from $C$–$V$ curves,[24] which confirms the thickness of $Al_2O_3$ to be 5 nm. In addition, for the MIS-capacitor, the plateau at 281 nF cm$^{-2}$ of the $C$–$V$ profile is consistent with the effective capacitance value considering series combination of an AlGaN barrier capacitance $C_{AlGaN}$ with relative permittivity of $\varepsilon_{AlGaN} = 9.2$ and a mist-$Al_2O_3$ capacitance due to $C_{Al_2O_3}$ capacitance with relative permittivity of $\varepsilon_{Al_2O_3} = 9$. Both samples exhibited very small hysteresis, which is particularly significant for the MIS-capacitor because it suggests excellent mist-$Al_2O_3$/AlGaN interfacial quality.[2,4] However, while the SG-capacitor showed a sudden decrease in capacitance due to leakage at positive applied voltage, the MIS-capacitor displayed a characteristic sudden second increase in capacitance with increasing voltage at around 0 V known as "spill-over", where some of the 2DEG from AlGaN/GaN quantum well spill over the $Al_2O_3$/AlGaN interface.[25] This spill-over phenomenon is hardly, if not at all, observable for poor insulator/semiconductor interfaces.[4,25,26]

The measured $C$–$V$ curve of MIS-capacitor was then fitted to one-dimensional simulation including self-consistent Poisson–Schrodinger calculations within the context of the DIGS model[19,20] proposed by Hasegawa and Ohno.[18] It is assumed in this model that disordered region on the semiconductor surface includes defects, dangling bonds and lattice displacements (bond lengths and angles disorders), thereby producing U-shape electronic states along the insulator/semiconductor interface with donor-like states below and acceptor-like states above the energy charge-neutrality level ($E_{CNL}$)].[18,27–30]

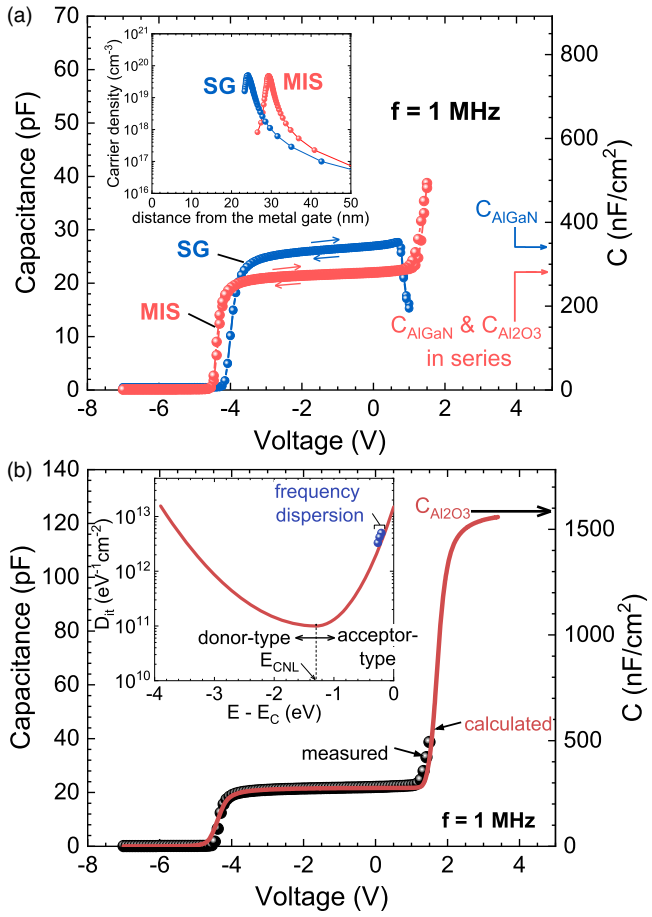


**Fig. 2.** (Color online) (a) Comparison of capacitance–voltage curves of SG- and MIS-capacitors measured at 1 MHz. Inset shows carrier density profiles derived from *C*–*V* curves. (b) Comparison between measured (solid circles) and calculated (solid line) *C*–*V* curves. Data points represent $D_{it}$ estimated from frequency dispersion method.

Figure 2(b) compares the measured (solid circles) and calculated *C*–*V* curves (solid line) at 1 MHz. By rigorous numerical fitting, we were able to adequately reproduce the measured *C*–*V* profile. In addition, U-shape $Al_2O_3$/AlGaN interface state density ($D_{it}$) distribution in accordance with the DIGS model were also extracted and indicated by the solid line in the inset, where a rather low interface state density of $1 \times 10^{11}\,eV^{-1}\,cm^{-2}$ at the $E_{CNL}$ was obtained. This $D_{it}$ minimum value is significantly lower even when compared to those of MIS-HEMTs reported in Ref. 20, which have undergone the post-metallization annealing process (PMA),[3,9,20,31] a process that has been recently gaining popularity for reducing $D_{it}$ along insulator/(Al)GaN interfaces. It should be pointed out that PMA is not yet performed on the present sample and will be the subject of our investigation in the future. Nevertheless, even the present results demonstrated the feasibility of as-deposited mist-$Al_2O_3$ for achieving high quality insulator/AlGaN interfaces suitable for device applications.

Figure 3 presents the frequency dependence of *C*–*V* profiles of the MIS-capacitor. The frequency dispersion is another way of estimating $D_{it}$ based on the fact that each frequency $f_n$ corresponds to an interface state energy depth $E_n$ given by the equation below:[32]

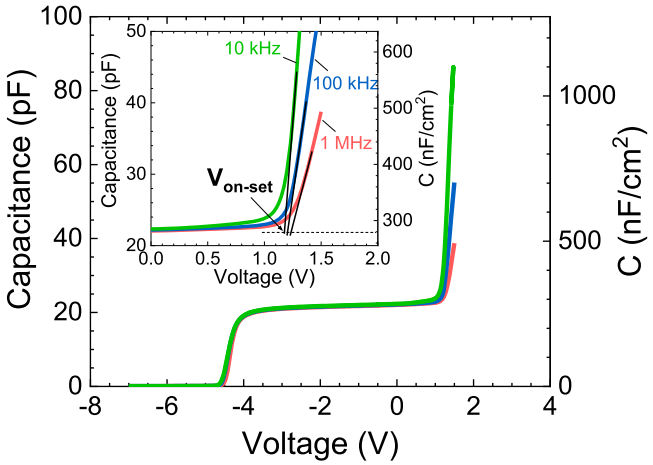


**Fig. 3.** (Color online) *C*–*V* curves of mist-$Al_2O_3$/AlGaN/GaN MIS-HEMT measured at frequencies of 10 kHz, 100 kHz, and 1 MHz. Inset shows zoomed-in region around spill-over regime.

$$E_n = kT \ln\left(\frac{\sigma N_C v_{th}}{2\pi f_n}\right). \tag{1}$$

Here, $k$ is the Boltzmann constant, $T$ is the temperature, $\sigma$ is the interface state capture cross-section, $N_C$ is the effective density of states at the conduction band edge, and $v_{th}$ is the electron thermal velocity. With increasing frequency, the on-set voltage ($V_{on\text{-}set}$) of the spill-over regime increases (see inset). The difference ($\Delta V_{on\text{-}set}$) between two values of $V_{on\text{-}set}$ corresponding to two measurement frequencies, and therefore to two interface state energies, can be used to estimate $D_{it}$ using the following equation]:[32]

$$D_{it}(E_{ave}) = \frac{C_{Al_2O_3}}{q} \times \left|\frac{\Delta V_{on\text{-}set}}{\Delta E}\right|, \tag{2}$$

where

$$\Delta E = E_2 - E_1 = kT \ln\left(\frac{\sigma N_C v_{th}}{2\pi f_2}\right) - kT \ln\left(\frac{\sigma N_C v_{th}}{2\pi f_1}\right) = kT \ln\left(\frac{f_1}{f_2}\right) \tag{3}$$

and

$$E_{ave} = E_1 + \frac{\Delta E}{2}. \tag{4}$$

In the equations above, $E_{ave}$ is the average, while $\Delta E$ is the difference energy, between two interface state energies corresponding to two measurement frequencies $f_1$ and $f_2$. The computed $D_{it}$ values using the *C*–*V* frequency dispersion technique, plotted as solid circles in the inset of Fig. 2(b), are in good agreement with those extracted from the earlier *C*–*V* curve fitting.

To determine and highlight the effects on the actual transistor device of a 5 nm thick mist-$Al_2O_3$ insertion between the gate metal and AlGaN layer, two-terminal gate leakage ($I_G$–$V_{GS}$), drain ($I_D$–$V_{DS}$), and transfer ($I_D$–$V_{GS}$) curves of the fabricated MIS-HEMTs were measured and compared with the reference SG-HEMT devices. Figure 4(a) shows the comparison of $I_G$–$V_{GS}$ of the devices, where the

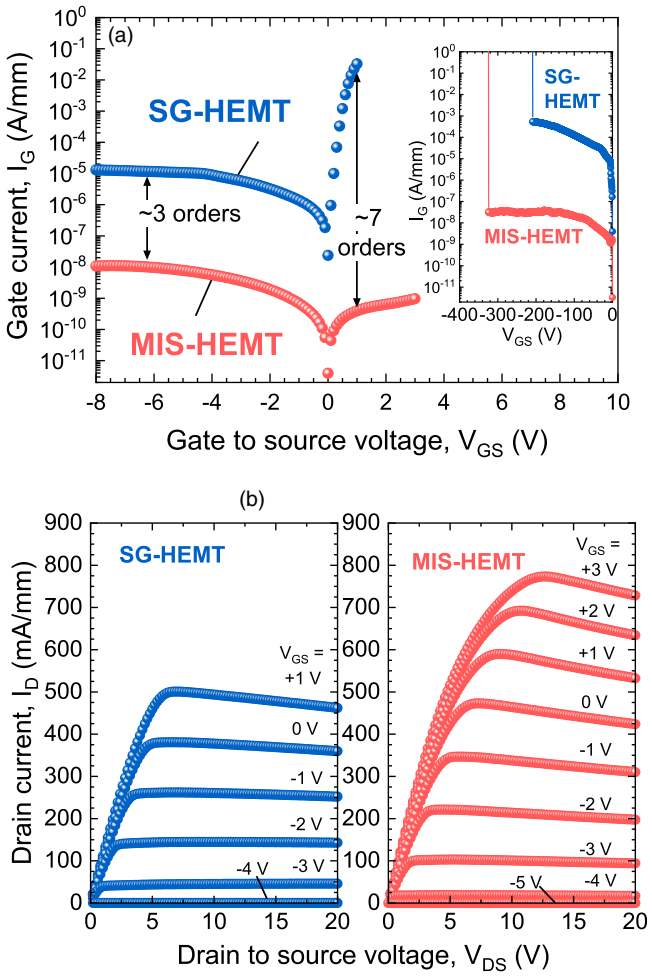


**Fig. 4.** (Color online) Comparison of (a) gate leakage characteristics of SG- and MIS-HEMTs. Inset shows reverse breakdown measurement results. (b) Drain curves of SG- and MIS-HEMTs.

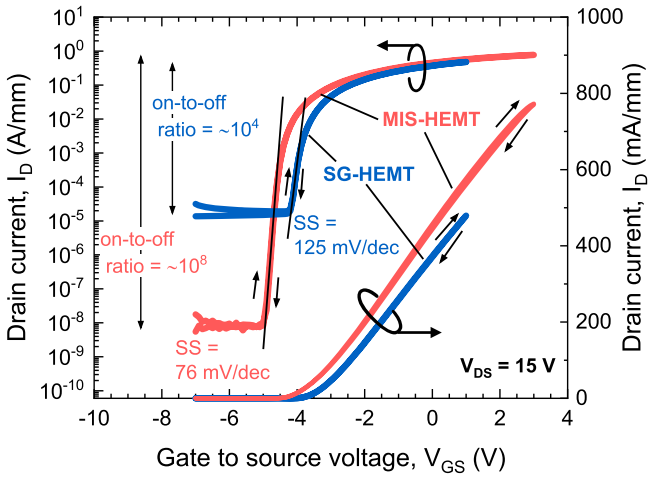


**Fig. 5.** (Color online) Comparison of dual-sweep $I_D$ versus $V_{GS}$ curves of SG- and MIS-HEMTs.

significantly lower leakage current in both negative and positive gate voltages was evident for the MIS-HEMT. At positive $V_{GS}$ of +1 V, in particular, a more than seven orders ($10^7$) of reduction was observed, suggesting highly suppressed forward gate leakage. This gate leakage mitigation in MIS-HEMT enables further increase of drain saturation current even at positive applied $V_{GS}$, and therefore can effectively lead to an increased input dynamic range. Reduction of leakage current via insertion of insulator material generally leads to improved device reverse breakdown voltage as discussed by Selvaraj et al.[33] As shown in the inset of Fig. 4(a), the MIS-HEMT showed a reverse breakdown voltage of 320 V compared with 210 V of SG-HEMT. This 50% increase in reverse breakdown voltage in MIS-HEMT suggests the suitability of mist-$Al_2O_3$ for power device applications. From the $I_D$–$V_{DS}$ curves presented in Fig. 4(b), both devices showed good drain output characteristics with complete pinch-off and saturation characteristics. Owing to the forward gate leakage mitigation in MIS-HEMT, a $V_{GS}$ of +3 V can be applied to the gate, boosting the maximum drain current to 780 mA $mm^{-1}$.

Figure 5 presents the comparison of dual-sweep semi-log and linear transfer curves for the MIS-HEMT and SG-HEMTs measured at $V_{DS}$ of 15 V. The threshold voltage ($V_{th}$) values, evaluated as the $V_{GS}$ required for $I_D$ to reach $1 \times 10^{-4}$ A $mm^{-1}$, were −4.1 V and −4.6 V for the SG- and MIS-HEMT devices, respectively. Similar to the SG-HEMT, the MIS-HEMT showed negligible hysteresis, verifying the excellent mist-$Al_2O_3$/AlGaN interfacial quality. Moreover, relative to its SG-HEMT counterpart, the MIS-HEMT exhibited more than 3 orders of magnitude increase in drain current on-to-off ratio. Furthermore, the MIS-HEMT has a much lower subthreshold swing SS of only 76 mV/dec, which compares well even with those record values reported in literature.[34] These results clearly demonstrate the viability of mist-CVD $Al_2O_3$ in the development of high-performance GaN-based MIS-HEMTs. For future work, we intend to investigate the large-area uniformity of our mist-CVD process and assess it scalability in production-like environments.

In summary, we have fabricated and characterized of AlGaN/GaN MIS-HEMTs using a 5 nm thick $Al_2O_3$ dielectric deposited by cost-effective and environmental-friendly mist CVD technique. Almost hysteresis-free capacitance–voltage profiles were obtained from the two-terminal MIS capacitors indicating high quality of the mist-$Al_2O_3$/AlGaN interface. Rigorous numerical fitting of the capacitance–voltage curves revealed a very low interface state density $D_{it}$ along the $Al_2O_3$/AlGaN interface of $1 \times 10^{11}$ $eV^{-1}$ $cm^{-2}$ at the charge neutrality level. Subsequent analyses of the measured frequency dispersion of capacitance–voltage profiles reproduced $D_{it}$ near the conduction band edge. MIS-HEMTs exhibited significantly improved performance such as much lower gate leakage current in both forward and reverse directions, higher drain maximum current, higher drain current on-to-off ratio, and lower subthreshold swing relative to Schottky-gate HEMTs. These results clearly demonstrated that mist-CVD $Al_2O_3$ is a promising greener alternative for the development of high-performance GaN-based MIS-HEMTs.

**Acknowledgments** This work was supported by JSPS KAKENHI Grant Numbers JP19H00761, JP19K04528, JP19K04473.

**ORCID iDs** Joel T. Asubar https://orcid.org/0000-0002-1829-4129 Zenji Yatabe https://orcid.org/0000-0003-2069-6677

1) M. Kuzuhara, J. T. Asubar, and H. Tokuda, Jpn. J. Appl. Phys. **55**, 070101 (2016).
2) Z. Yatabe, J. T. Asubar, and T. Hashizume, J. Phys. D **49**, 393001 (2016).

3) T. Hashizume, K. Nishiguchi, S. Kaneki, J. Kuzmik, and Z. Yatabe, Mater. Sci. Semicond. Proc. **78**, 85 (2018).
4) Z. Yatabe, Y. Hori, W. Ma, J. T. Asubar, M. Akazawa, T. Sato, and T. Hashizume, Jpn. J. Appl. Phys. **53**, 100213 (2014).
5) G. He, X. Wang, M. Oshima, and Y. Shimogaki, Jpn. J. Appl. Phys. **49**, 031502 (2010).
6) K. Yoshitsugu, M. Horita, Y. Ishikawa, and Y. Uraoka, Phys. Status Solidi C **10**, 1426 (2013).
7) S. P. Le, D. D. Nguyen, and T. Suzuki, J. Appl. Phys. **123**, 034504 (2018).
8) J. Yang, B. S. Eller, M. Kaur, and R. J. Nemanich, J. Vac. Sci. Technol. A **32**, 21514 (2014).
9) S. Kaneki, J. Ohira, S. Toiya, Z. Yatabe, J. T. Asubar, and T. Hashizume, Appl. Phys. Lett. **109**, 162104 (2016).
10) Y. Xiang, C. Zhou, E. Jia, and W. Wang, Nanoscale Res. Lett. **10**, 137 (2015).
11) H. Tokuda, J. T. Asubar, and M. Kuzuhara, Jpn. J. Appl. Phys. **55**, 120305 (2016).
12) K. Aikawa and S. Fujita, Jpn. J. Appl. Phys. **51**, 070203 (2012).
13) T. Kawaharamura, T. Uchida, M. Sanada, and M. Furuta, AIP Adv. **3**, 032135 (2013).
14) G. T. Dang, M. W. Allen, M. Furuta, and T. Kawaharamura, Jpn. J. Appl. Phys. **58**, 090606 (2019).
15) T. Uchida, T. Kawaharamura, K. Shibayama, T. Hiramatsu, H. Orita, and S. Fujita, Appl. Phys. Express **7**, 021303 (2014).
16) Z. Yatabe, K. Nishiyama, T. Tsuda, and Y. Nakamura, J. Ceram. Soc. Jpn. **127**, 590 (2019).
17) Z. Yatabe, K. Nishiyama, T. Tsuda, K. Nishimura, and Y. Nakamura, Jpn. J. Appl. Phys. **58**, 07095 (2019).
18) H. Hasegawa and H. Ohno, J. Vac. Sci. Technol. B **4**, 1130 (1986).
19) M. Miczek, C. Mizue, T. Hashizume, and B. Adamowicz, J. Appl. Phys. **103**, 104510 (2008).
20) K. Nishiguchi, S. Kaneki, S. Ozaki, and T. Hashizume, Jpn. J. Appl. Phys. **56**, 101001 (2017).
21) T. Hashizume and H. Hasegawa, Appl. Surf. Sci. **234**, 387 (2004).
22) R. S. Low, S. Kawabata, J. T. Asubar, H. Tokuda, and M. Kuzuhara, IEEE IMFEDK Tech. Dig., 2019, p. 77.
23) Z. Yatabe, T. Tsuda, J. Matsushita, T. Sato, T. Otabe, K. Sue, S. Nagaoka, and Y. Nakamura, Phys. Status Solidi C **14**, 1600148 (2017).
24) C. O. Thomas, D. Kahng, and R. C. Manz, J. Electrochem. Soc. **109**, 1055 (1962).
25) C. Mizue, Y. Hori, M. Miczek, and T. Hashizume, Jpn. J. Appl. Phys. **50**, 021001 (2010).
26) J. T. Asubar, S. Kawabata, H. Tokuda, A. Yamamoto, and M. Kuzuhara, IEEE Electron Device Lett. **41**, 693 (2020).
27) M. Miczek, B. Adamowicz, C. Mizue, and T. Hashizume, Jpn. J. Appl. Phys. **48**, 04C092 (2009).
28) B. Bakeroot, S. You, T.-L. Wu, J. Hu, M. Van Hove, B. De Jaeger, K. Geens, S. Stoffels, and S. Decoutere, J. Appl. Phys. **116**, 134506 (2014).
29) M. Matys, S. Kaneki, K. Nishiguchi, B. Adamowicz, and T. Hashizume, J. Appl. Phys. **122**, 224504 (2017).
30) M. Ťapajna et al., Appl. Surf. Sci. **426**, 656 (2017).
31) Y. Ando, S. Kaneki, and T. Hashizume, Appl. Phys. Express **12**, 024002 (2019).
32) Y. Hori, Z. Yatabe, and T. Hashizume, J. Appl. Phys. **114**, 244503 (2013).
33) S. L. Selvaraj, T. Ito, Y. Terada, and T. Egawa, Appl. Phys. Lett. **90**, 173506 (2007).
34) H. Tokuda, J. T. Asubar, and M. Kuzuhara, Jpn. J. Appl. Phys. **56**, 104101 (2017).